Exploring the $OH+CO \rightarrow H+CO_2$ potential surface via dissociative photodetachment of $(HOCO)^-$

Todd G. Clements and Robert E. Continetti[a)]
Department of Chemistry and Biochemistry, University of California, San Diego, La Jolla, California 92093-0340

Joseph S. Francisco
Department of Chemistry and Department of Earth and Atmospheric Sciences, Purdue University, West Lafayette, Indiana 47907-1393

(Received 15 May 2002; accepted 17 July 2002)

Dissociative photodetachment (DPD) of the molecular anion $HOCO^-$ is used to probe the potential energy surface for the $OH+CO \rightarrow H+CO_2$ reaction. The $HOCO^-$ anion, formed by electron impact on an expansion of CH_4+N_2O+CO, is characterized for the first time in these experiments by photoelectron spectroscopy and photoelectron angular distribution measurements. Photodetachment of $HOCO^-$ is found to produce $H+CO_2+e^-$ and $OH+CO+e^-$ products in addition to stable HOCO radicals. *Ab initio* calculations of the energetics and structure of $HOCO^-$ and HOCO are consistent with the experimental results and show that photodetachment to the ground electronic HOCO surface samples the vicinity of the HOCO well. The product translational energy distributions observed on the ground state surface are consistent with unimolecular decomposition out of the HOCO well. In addition, direct DPD to a repulsive excited state of HOCO, correlating to ground state $OH+CO$ products is observed. © *2002 American Institute of Physics.*
[DOI: 10.1063/1.1505439]

I. INTRODUCTION

The $OH+CO \rightarrow H+CO_2$ reaction plays an important role in the production of CO_2 in combustion processes[1] and the tropospheric chemistry of the hydroxyl radical,[2] and has thus been the subject of a number of experimental and theoretical studies. It has been shown that a HOCO intermediate plays an important role in the reaction, and in recent years focus on the potential energy surface and dynamics of this reaction has increased. In the experiments presented here, dissociative photodetachment of the $HOCO^-$ anion is used to provide insight into the potential energy surface and dynamics of this important reaction.

Experimental studies of the dynamics of this reaction have focused on reactive and nonreactive scattering of $OH+CO$ (Ref. 3) or $H+CO_2$ coupled with state-resolved measurement of product distributions.[4–7] Additionally, half-collision dynamics have been probed through the use of XHOCO (X=Br,I) van der Waals precursors.[8–10] The scattering experiments of Alagia *et al.*[3] and Brouard *et al.*[7] showed that the lifetime of the reactive collision complexes formed in the bimolecular reaction is on the order of the rotational period of the complex, allowing intramolecular vibrational redistribution (IVR) to take place before dissociation. Recently, Lester and co-workers have examined the potential energy surfaces for this reaction by spectroscopically characterizing a hydrogen-bonded OH–CO entrance-channel complex.[11] The HOCO well has also been spectroscopically characterized by rotational and vibrational spectroscopic measurements.[12,13] Previously, the most stable isomer of neutral HOCO has been shown via matrix-isolation studies to be the *trans* isomer,[14] although calculations show that the difference in energy between the *cis* and *trans* isomers is small, 0.09 eV at the CBS-QB3 level of theory.[15] The energetics of HOCO continue to be experimentally refined as shown in the recent photoionization study of Ruscic and Litorja finding a lower limit for $\Delta H^0_{f0}(trans\text{-HOCO}) \geqslant 1.99 \pm 0.03$ eV.[16]

The potential energy surface (PES) and dynamics governing this reaction have been the subject of considerable theoretical[17–22] investigation as well, and with the extension of *ab initio* quantum dynamics calculations to systems with more degrees of freedom, calculation of the six-dimensional PES and dynamics on that surface are becoming tractable. There have already been full-dimensionality calculations of the dynamics for this system,[23] including the recent fully converged quantum calculations of McCormack and Kroes.[24] Recently, the *ab initio* calculations have been extended to excited states in the work of Li and Francisco[25] and a new six-dimensional analytic potential energy surface has been reported by Yu, Muckerman, and Sears.[26]

To the best of our knowledge, there have been no previous experimental or theoretical studies of the $HOCO^-$ molecular anion, although the isomeric formate anion, HCO_2^-, has received attention. Photoelectron spectroscopy experiments by Neumark and co-workers[27] characterized the electron affinity and energetics of the low-lying excited states of the formyloxyl radical, HCO_2. Clements and Continetti studied the dissociative photodetachment (DPD) dynamics of the HCO_2^- and DCO_2^- anions,[28] providing insights into the predissociation dynamics of the radicals following photode-

a)Author to whom correspondence should be addressed. Electronic mail: rcontinetti@ucsd.edu

tachment using photoelectron–photofragment coincidence (PPC) spectroscopy. In those experiments, state-resolved translational energy distributions were observed correlated to OCO bending excitation in the CO_2 product with very little product rotation, but no evidence was found for formation of $OH+CO$ products. In the experiments reported here, the isomeric $HOCO^-$ anion was formed by the reaction of OH^-+CO in a supersonic expansion, yielding an anion with a distinct photoelectron spectrum and dissociation pathways.

These experiments represent an ideal application of photoelectron–photofragment coincidence (PPC) spectroscopy. For stable or metastable intermediates such as HOCO where the anionic and neutral geometries differ, photodetachment of an anionic precursor can create a neutral molecule displaced from the minimum of the neutral potential well, allowing exploration of a different portion of the neutral potential surface than bimolecular reactions or studies employing a neutral precursor complex. At the energies employed in this study, $HOCO^-$ can undergo DPD via two pathways,

$$HOCO^- + h\nu \rightarrow OH + CO + e^-, \quad (1)$$

$$HOCO^- + h\nu \rightarrow H + CO_2 + e^-. \quad (2)$$

The present study reports PPC experiments, including photoelectron coincidence imaging measurements of photoelectron angular distributions, on the DPD of $HOCO^-$. These experiments give insight into the dynamics of HOCO dissociation and the energetics and electronic structure of the parent anion. To complement the experimental results, the first calculations of the geometry and energetics of the $HOCO^-$ molecular anion are also presented. The results are qualitatively consistent with dynamics expected on the potential surface governing the reaction $OH+CO \rightarrow HOCO^* \rightarrow H+CO_2$, and provide the basis for future tests of dynamical theories.

II. EXPERIMENT

The two photoelectron–photofragment coincidence spectrometers employed in these studies have been described in detail previously, and will be only briefly reviewed here.[29,30] The $HOCO^-$ anion was produced using two methods. Ions were created either by intersecting a 1 keV electron beam with a supersonic expansion of 23% CO, 20% N_2O, and 57% CH_4 or by using a pulsed discharge on the supersonic expansion. Anions were accelerated to 4–7 keV and rereferenced to ground by a high-voltage potential switch operated at 1 kHz. Anions with $m/e=45$ were mass selected by time-of-flight and guided into an interaction region where they were intersected by either the second (388 nm, 3.20 eV) or third (258 nm, 4.80 eV) harmonic of a linearly polarized Ti:Sapphire laser (1.4 ps FWHM Clark CPA-2000).

Photoelectron images at 258 and 388 nm were obtained using a spectrometer with a space focusing electron optics assembly.[31,32] Roughly 150 ns before photodetachment, a 16 V/cm extraction field is applied in the interaction region. The use of this extraction field allows for collection of the full 4π sr of the photodetached electrons. The extracted electrons pass through a grid, fly through a field free region, pass through a second grid and are then accelerated onto a time- and position-sensitive detector. The photoelectron image is thus obtained directly, and the full three-dimensional electron distribution can be recreated directly from the data using the electron time-of-flight information. However, due to the required timing resolution, the CM eKE resolution using this technique is reduced to $\Delta E/E \approx 15\%$ as shown in experiments on the photodetachment of O^- at 388 nm and I^- at 258 nm.

The DPD experiments at 258 nm were carried out using the electron impact source and a separate spectrometer employing two opposed time- and position-sensitive straight time-of-flight photoelectron detectors that collect roughly 10% of the 4π sr solid angle of the photodetached electrons. The time and position information is used to correct for the large Doppler shift arising from the fast ion beam. Using the photodetachment of I^- at 258 nm, the center-of-mass (CM) electron kinetic energy (eKE) resolution was determined to be $\Delta E/E \approx 7\%$ at 0.8 eV and 7 keV beam energy. The photoelectron spectrum of OH^- reported in this paper shows a FWHM of 0.24 at 2.98 eV, indicating a resolution of 8% $\Delta E/E$ at 2.98 eV and 7 keV beam energy.

Neutral photofragments recoil out of the fast beam, and impinge on a four quadrant multiparticle time- and position-sensitive microchannel-plate-based detector. Each quadrant is capable of detecting up to two particles per dissociation event as long as the particles are separated by more than the ~15 ns dead time of the detector electronics. Conservation of momentum and the time and position information are used to determine the photofragment mass ratio and subsequently the CM kinetic energy release (E_T) of the neutral particles. Using the photodissociation of O_2^-, the CM E_T resolution of the detector was determined to be $\Delta E/E \approx 11\%$ at $E_T = 0.70$ eV and 7 keV beam energy. The photofragment E_T spectrum was also measured using the photoelectron imaging apparatus to aid in verifying that the same ion was being produced in both experiments. The two-particle detector on this instrument has a significantly smaller detector acceptance function (DAF). In order to correct for the DAF and approximate the actual translational energy distribution, $P(E_T)$, from the measured distribution, $N(E_T)$, Monte Carlo simulations of the apparatus and dissociation dynamics were employed. For a simulation of each apparatus, a large number of trajectories were run where each dissociation event had an equal $P(E_{T,\mathrm{MC}})$ and an isotropic angular distribution from 0 to 2 eV. Those events where one particle landed outside the detector region, or were otherwise undetectable (such as two particles hitting one detector within the 15 ns dead time) were discarded. The resulting $N(E_{T,\mathrm{MC}})$ distribution was divided into the experimental $N(E_T)$ distribution to yield an approximate $P(E_T)$.[33] After correction for the significantly smaller DAF on the photoelectron imaging apparatus, the E_T spectrum obtained from the two spectrometers exhibited the same features and relative intensities except at very low E_T ($E_T \leqslant 0.05$ eV), where the photofragment detector on the photoelectron imaging apparatus has essentially zero detection efficiency given the kinematics and dynamics of this system. False coincidences were minimized by carrying out the experiments at an average detachment rate of 0.032 events per laser shot. Regardless of the actual branch-

TABLE I. Optimized geometries for HOCO neutral and anion at the CCSD(T) level of theory with several basis sets. Bond lengths are given in Å and bond angles are given in deg.

Species	Method	Bond lengths			Bond angles	
		HO′	CO′	CO	HO′C	OCO′
HOCO($X\,^2A'$) *cis*	CCSD(T)/6-31G(d)	0.986	1.343	1.199	107.9	129.7
	CCSD(T)/6-31+G(d)	0.988	1.342	1.199	108.7	130.0
	CCSD(T)/6-311G($3df$,$3pd$)	0.971	1.331	1.184	107.7	130.2
	CCSD(T)/6-311++G($3df$,$3pd$)	0.973	1.331	1.185	107.9	130.4
HOCO($X\,^2A'$) *trans*	CCSD(T)/6-31G(d)	0.976	1.358	1.194	107.5	126.4
	CCSD(T)/6-31+G(d)	0.977	1.357	1.193	108.2	126.7
	CCSD(T)/6-311G($3df$, $3pd$)	0.962	1.345	1.179	107.4	126.8
	CCSD(T)/6-311++G($3df$,$3pd$)	0.961	1.344	1.180	107.6	127.1
$HOCO^-$($X\,^1A'$) *cis*	CCSD(T)/6-31G(d)	0.988	1.493	1.250	100.3	108.7
	CCSD(T)/6-31+G(d)	0.993	1.462	1.245	103.3	111.4
	CCSD(T)/6-311G($3df$,$3pd$)	0.973	1.469	1.231	100.3	110.2
	CCSD(T)/6-311++G($3df$,$3pd$)	0.977	1.450	1.231	102.2	111.9
$HOCO^-$($X\,^1A'$) *trans*	CCSD(T)/6-31G(d)	0.975	1.595	1.226	98.5	108.2
	CCSD(T)/6-31+G(d)	0.977	1.517	1.227	101.3	110.6
	CCSD(T)/6-311G($3df$,$3pd$)	0.957	1.549	1.211	98.5	109.5
	CCSD(T)/6-311++G($3df$,$3pd$)	0.961	1.506	1.214	100.3	110.8

ing ratios, owing to the low collection and detection efficiency for the H atom, significantly less data is available for the $H+CO_2$ channel. Monte Carlo simulations indicate that $\approx$7% of the $H+CO_2$ photofragment pairs strike the detector, and a detection efficiency of only $\approx$0.1 for H atoms in the 100–200 eV laboratory energy range with a microchannel-plate detector has been recently reported.[34]

III. CALCULATIONS

Theoretical calculations were performed using the GAUSSIAN 98 suite of programs.[35] Geometries were optimized using the coupled cluster CCSD(T) method including single, double, and triple excitations[36] with the Pople basis set (6-31G(D)), both with and without polarization and diffuse functions.[37] The method and basis set were chosen to be consistent with previous work on the $HOCO^+$ system.[38] Table I shows the results of the geometry calculations for several different basis sets at the CCSD(T) level of theory. A comparison of geometries between augmented and unaugmented basis sets shows that very little change is calculated for the basis sets used for the neutral. However, all basis sets show a large change in geometry between the anionic and neutral forms of HO′CO. It should be noted that the largest geometric effect of the diffuse functions is on the geometry with the smaller 6-31G(d) basis set. For example, there is a 0.029 Å difference in the CO′ bond for the *cis* anionic structure. This is significantly reduced to 0.019 Å with the 6-311G($3df$,$3pd$) basis set. This difference is even more exaggerated with the *trans* anionic structure. For example, the difference between 6-31G(d) and 6-31+G(d) results for the CO′ bond is 0.078 Å and reduced to 0.043 Å with the larger basis set. These results suggest that both the diffuse functions and the large basis sets are needed to describe the geometry of the HOCO anion. The geometry change is mainly in the two bond angles and the central CO bond distance, which decreases by 0.16 Å from the *trans*-anion to the *trans*-neutral using the 6-311++G($3df$,$3pd$) basis set. In both the *trans* and *cis* isomers, the neutral optimized to a more open structure (larger bond angles) than the anion. Moreover, the CO bonds in the anionic structures are all lengthened.

Frequencies were calculated using the CCSD(T)/6-31G(d) method and basis set and are presented in Table II. The results for the *trans*-HOCO isomer are the same as reported previously by Francisco[38] and show good agreement with experimental frequencies as shown in the

TABLE II. Vibrational frequencies, in cm^{-1}, for the HOCO neutral and anion at the CCSD(T)/6-31G(d) level of theory.

Mode	Symmetry	HOCO *cis*	HOCO *trans*	$HOCO^-$ *cis*	$HOCO^-$ *trans*	Expt. (HOCO *trans*)
O′H stretch	a'	3352	3726	3452	3665	3603,[a] 3635[b]
C–O stretch	a'	1867	1903	1623	1713	1844,[a] 1843.7[c]
HO′C bend	a'	1330	1280	1204	1087	1211[a]
C–O′ stretch	a'	1093	1089	741	663	1065[a]
O′CO bend	a'	595	606	532	402	615[a]
torsion	a''	599	540	710	485	515

[a]Reference 52.
[b]Reference 13.
[c]Reference 12.

TABLE III. Total and relative energies for *cis* and *trans* HOCO neutral and anion.

	CCSD(T)				
Total energies (hartrees)	6-31G(d)	6-31+G(d)	6-311G($3df$,$3pd$)	6-311++G($3df$,$3pd$)	ZPE(6-31G(d))
CO	−113.038 19	−113.046 04	−113.154 08	−113.156 69	0.004 91
OH^-	−75.521 83	−75.593 56	−75.659 38	−75.699 64	0.007 72
HOCO, *cis*	−188.611 75	−188.626 26	−188.832 24	−188.837 97	0.020 59
HOCO, *trans*	−188.613 18	−188.629 04	−118.834 83	−188.840 92	0.020 83
$HOCO^-$, *cis*	−188.620 56	−188.672 71	−188.865 04	−188.888 82	0.018 82
$HOCO^-$, *trans*	−188.613 66	−188.670 23	−188.861 37	−188.886 27	0.018 26
cis isomers					
Dissociation energy[a] (eV)	1.48	0.73	1.23	0.72	
AEA (eV)	0.29	1.31	0.94	1.43	
Trans isomers					
Dissociation energy[a] (eV)	1.31	0.68	1.15	0.66	
AEA (eV)	0.08	1.19	0.79	1.30	
ΔE (*cis*, *trans* anion, eV)	0.17	0.05	0.08	0.05	

[a]$HOCO^- \rightarrow OH^- + CO$.

table. It is interesting to compare the geometry of *cis*-HOCO neutral and the *cis*-$HOCO^-$ anion. In the *cis*-$HOCO^-$ anion, the CO bond length increases by 0.051 Å in the CCSD(T)/6-31G(d) calculations, suggesting that the CO stretching mode should decrease in frequency because of the weakened bond. A comparison of the frequencies in Table II shows a shift of 244 cm^{-1} to lower frequency for this CO stretching mode. A similar trend is seen in the shift of the CO stretching mode frequency in the $HOCO^-$ *trans* anion, consistent with the structural changes. The CO′ bond in both *cis*- and *trans*-$HOCO^-$ structures are very elongated and showed the largest red shift in the vibrational frequency for the C–O′ stretch. There is a 352 cm^{-1} shift for the *cis* C–O′ stretch and a 421 cm^{-1} shift for the *trans* C–O′ stretch in the HOCO anionic structures.

Table III shows total energies for the anionic and neutral forms of both isomers of HOCO, as well as the anion dissociation energy $HOCO^- \rightarrow OH^- + CO$ and the adiabatic electron affinity (AEA). The zero point energy (ZPE) calculated at the 6-31G(d) level was used to correct the energy calculations, including the binding energy and the adiabatic electron affinity, at all levels of theory. Table III shows that in calculations of the binding energy and adiabatic electron affinity, diffuse functions are necessary in order to obtain accurate energetics for the $HOCO^-$ anion, as expected. Surprisingly, the energy difference between CCSD(T)/6-31+G(d) and CCSD(T)/6-311++G($3df$,$3pd$) results are small, i.e., <25 meV for the dissociation energy. There is a 120 meV difference in the adiabatic electron affinity, but this difference is still very reasonable. Based on calibration calculations with HCO^-, the uncertainty in the calculated adiabatic electron affinity energy is ±0.07 eV. Thus, the results for the $HOCO^-$ anion calculated at the CCSD(T)/6-311++G($3df$,$3pd$) level should be reliable.

IV. RESULTS

A. Photoelectron–photofragment coincidence spectra

The photoelectron–photofragment coincidence spectra, $N(E_T,\text{eKE})$, for both DPD reactions (1) and (2) are shown in Fig. 1. These spectra reveal how the photoelectron and photofragment translational energy distributions are correlated. Each point in the two-dimensional histogram represents an event with a given correlated eKE and E_T. The $N(E_T)$ and $N(\text{eKE})$ spectra shown along the x and y axes are generated by integrating over the complementary variable in the spectrum.

The sets of diagonal lines on the spectra show energetic limitations for DPD of $HOCO^-$ into the two observed product channels, (1) $OH+CO+e^-$ and (2) $H+CO_2+e^-$. The closely spaced sets of lines correspond to the theoretically predicted energetics for the *cis*- and *trans*-$HOCO^-$ anions, as we have no firm basis for discriminating which of these nearly isoenergetic isomers are present in the beam. For both the $OH+CO$ and $H+CO_2$ product channels, the diagonal lines (I) represent the maximum total energy, KE_{MAX}, available for DPD producing ground electronic and vibrational state products. For the $OH+CO+e^-$ channel, the limit was calculated using the CCSD(T)/6-311++G($3df$,$3pd$) results and the electron affinity of OH,[39] yielding $KE_{MAX}=2.26$, 2.31 eV for *cis*- and *trans*-$HOCO^-$, respectively. The energetic limits, $KE_{MAX}=3.31$, 3.36 eV, for the DPD of *cis*- and *trans*-$HOCO^-$, respectively, to $H+CO_2+e^-$ are given by the theoretical results for the $OH+CO+e^-$ channel and the experimental enthalpy for the reaction $OH+CO \rightarrow H+CO_2$ at 0 K.[40] On the $OH+CO+e^-$ spectrum, line (II) represents the maximum available energy (3.37, 3.50 eV) from the theoretical calculations for photodetachment from *cis*- or *trans*-$HOCO^-$ to the bottom of the *cis*- or *trans*-HOCO wells, respectively.

Qualitatively, the spectra indicate that in the $H+CO_2+e^-$ channel there are two possible dissociation pathways, one with a significant E_T (0.53 eV), as seen in the $P(E_T)$ distribution. The second feature, at very low E_T, is proposed to arise from false coincidences with stable HOCO radicals in the beam. The $OH+CO+e^-$ channel exhibits three main features. The first is a very low E_T, high eKE region. Given the high eKE, this region might result from photodetachment of bare or perturbed OH^-. However, the photoelectron imaging studies discussed below preclude the presence of ionic photodissociation or weakly bound $OH^-(CO)$, so this region

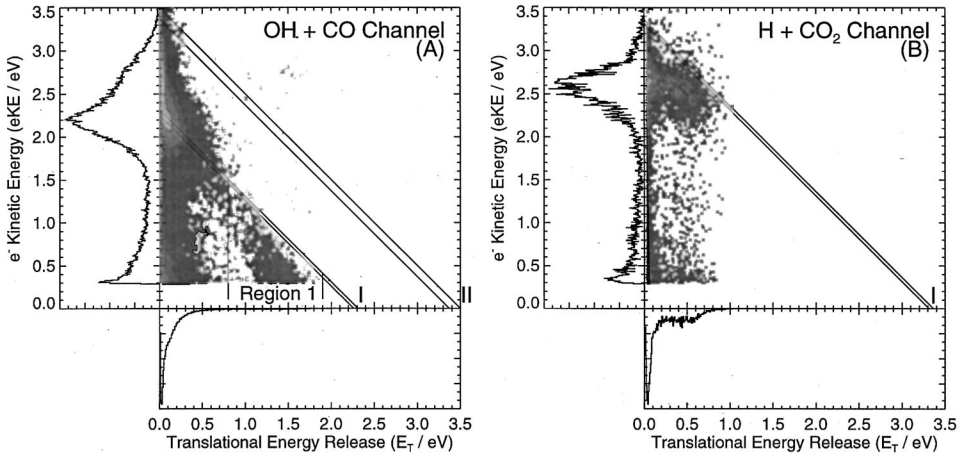

FIG. 1. Photoelectron–photofragment correlation spectrum, $N(E_T,\mathrm{eKE})$, for the dissociative photodetachment of $HOCO^-$ at 258 nm producing $H+CO_2+e^-$ and $OH+CO+e^-$. Each point represents the correlated photoelectron kinetic energy and photofragment translational energy release for a DPD event. The diagonal lines (I) in each figure corresponds to the maximum kinetic energy release for production of ground state neutral products calculated at the CCSD(T)/6-311++G($3df$,$3pd$) level of theory for *cis*- and *trans*-$HOCO^-$ anions as discussed in the text. The diagonal lines (II) in (A) corresponds to the maximum kinetic energy release for photodetachment of $HOCO^-$ to the minimum of the neutral well. Region 1 corresponds to the high E_T portion of the OH+CO spectrum, originating from direct DPD on a repulsive excited state.

is concluded to result from false coincidences with stable HOCO radicals as observed in the $H+CO_2$ channel. The second region is at intermediate E_T and lower eKE, with a tail extending out to $E_T \approx 0.6$ eV. Finally, a region at high E_T, seen as a diagonal band along limit I, correlating to ground state $OH+CO+e^-$ products is denoted as region 1 on the figure. This last feature is consistent with direct DPD on a repulsive surface, as previously observed for O_4^-, $O^-(H_2O)$, and $OH^-(H_2O)$.[41–43]

Both product channels show a peak at low E_T and high eKE, however the intensity of this feature is much higher in the $OH+CO+e^-$ data. As discussed above, this feature is assigned to false coincidences involving detection of stable $HOCO+e^-$ and a single fragment (OH, CO, or CO_2) from either of the dissociation channels. Usually false coincidences of this type are rejected since they do not conserve momentum. However, as E_T approaches zero, this test fails. The false coincidence contribution to the $H+CO_2$ channel is reduced because the momentum conservation constraints for these mass ratio (1:44) products is more effective even at very low energies in discriminating against false coincidences involving a stable HOCO radical. In the following sections, the photoelectron and photofragment translational spectra contained in these correlation spectra are examined in greater detail.

B. Photoelectron spectra

Photoelectron spectra, $N(\mathrm{eKE})$, for $HOCO^-$ obtained at 258 nm are shown in Fig. 2. Since these spectra are acquired in coincidence with two neutral photofragmentation channels there are several spectra displayed to illustrate the nature of the photoelectron spectrum for this species. In the bottom frame four spectra are shown. The narrowest spectrum, peaking at 2.98 eV (with a FWHM of 0.24 eV), is the photoelectron spectrum of OH^-, providing a measure of the energy resolution of the spectrometer. The lower energy spectrum, peaking at 2.2 eV, is the spectrum of photoelectrons obtained in coincidence with $OH+CO$ photofragments as seen in Fig. 1(A), and the higher energy spectrum peaking at 2.60 eV is for photoelectrons obtained in coincidence with $H+CO_2$ photofragments as seen in Fig. 1(B). The photoelectron spectrum for the $H+CO_2+e^-$ channel is consistent with a perturbed OH^- spectrum, implying the possible existence of a weakly bound $OH^-(CO)$ complex. As mentioned previously, this possibility is discounted by examination of the photoelectron angular distributions. The fourth spectrum is the solid line peaking at 2.68 eV scaled to the $OH+CO+e^-$ spectrum. This spectrum is generated from photoelectrons coincident with a single particle (predominantly stable

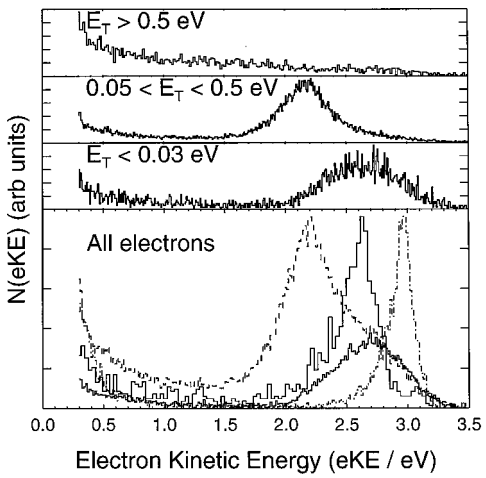

FIG. 2. Photoelectron spectra, $N(\mathrm{eKE})$, for $HOCO^-$ obtained at 258 nm (4.80 eV). In the bottom frame, the dashed line is the spectrum for photoelectrons obtained in coincidence with $OH+CO$ photofragments, the tall solid line for photoelectrons obtained in coincidence with $H+CO_2$ photofragments, and the dotted–dashed line is the photoelectron spectrum for OH^-, shown for reference. The small solid feature under the $OH+CO$ photoelectron spectrum corresponds to stable HOCO radicals as discussed in the text. The upper three panels show differential photoelectron spectra for specific E_T ranges in the $OH+CO+e^-$ DPD channel.

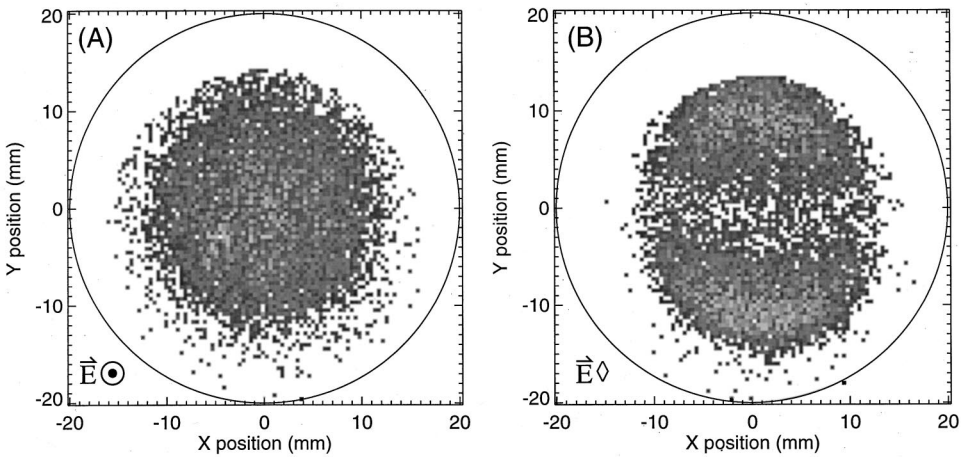

FIG. 3. Photoelectron images of the photodetachment of $HOCO^-$ obtained at 388 nm. (A) Photoelectron image with the laser polarized perpendicular to the detector face. (B) Photoelectron image with the laser polarized parallel to the detector face. The direction of the ion beam is from the bottom to the top of the images.

HOCO or one of the CO_2 products from the $H+CO_2$ channel) hitting the detector within a spherical radius of 2 mm from the nominal time- and position-of-arrival of the parent beam. The spherical gating on the photoelectron data recorded in coincidence with a single particle is most effective at removing contributions from dissociative channels. The good fit of the spherically gated spectrum to the shoulder on the $OH+CO$ spectrum supports the assignment of this feature to false coincidences with stable $HOCO+e^-$ products as discussed above. All spectra show a cutoff at eKE $=0.3$ eV, below which background electrons from the laser striking surfaces inside the spectrometer dominate the spectrum.

Also shown in Fig. 2 are photoelectron spectra correlated with specific E_T ranges for $OH+CO+e^-$ products. These spectra show a significant relationship between eKE and E_T as seen in the correlation spectrum. In the top frame, those electrons correlated with very high E_T neutrals ($E_T > 0.5$ eV) exhibit a broad spectrum, and would likely not be notable were it not for the distinct coincident feature in observed in the correlation spectrum in region 1. In the second frame from the top, the electrons correlated with E_T between 0.05 and 0.5 eV show a narrower spectrum peaking at 2.2 eV as observed in the summed $OH+CO+e^-$ photoelectron spectrum in the bottom frame. Finally, in the third frame from the top, a distinct photoelectron spectrum peaking at 2.7 eV is observed for extremely low ($E_T < 0.03$ eV) energy $OH+CO$ neutrals. This spectrum is nearly identical to the spherically gated single particle photoelectron spectrum discussed in the previous paragraph and is a result of photodetachment to stable HOCO radicals.

Figure 3 shows the photoelectron images obtained at 388 nm on the photoelectron imaging apparatus. The images show clear anisotropy in the angular distribution of the photodetached electrons, with similar results obtained at 258 nm. With the laser polarized parallel to the detector face, two lobes appear along the direction of the electric vector, indicating a $\cos^2(\theta)$ distribution. The three-dimensional velocity distributions represented by these two-dimensional photoelectron images can be used to obtain the anisotropy parameter, β, for photodetachment of $HOCO^-$, given by the following formula:

$$\frac{\partial\sigma}{\partial\Omega} = \frac{\sigma_{\text{total}}}{4\pi}[1+\beta(E)P_2(\cos\theta)], \tag{3}$$

where σ_{total} is the total photodetachment cross section, $P_2(\cos\theta)$ is the second-order Legendre polynomial in $\cos\theta$, and $\beta(E)$ is the energy-dependent anisotropy parameter.[44] A common technique employed to extract β from photoelectron images is the Abel transform.[45–48] This is necessary in order to determine three-dimensional angular distributions from the two-dimensional images, assuming cylindrical symmetry around the electric vector of the laser. With the coincidence imaging technique both the time and position of arrival of each electron is measured yielding a true three-dimensional representation of the electron image. As a result, the photoelectron angular distribution (PAD) is contained directly in the data, and β is easily determined. Using this method, β is determined to be 1.2 ± 0.2 averaged over all photoelectron energies, consistent with *p*-wave photodetachment. The same value for β was determined using both the pulsed discharge and electron impact ion sources, providing further evidence that the same ions were produced in both sources.

These results can be compared to the PADs for OH^-, to rule out the occurrence of ionic photodissociation of $HOCO^-$ followed by photodetachment of the OH^- product or the presence of a weakly bound $OH^-(CO)$ cluster in the beam. At 351 nm, photodetachment from OH^- produces an electron with $\beta=-0.64$, showing *d*-wave photodetachment.[49] At 388 nm a value of $\beta=-0.7\pm0.2$ was found for OH^-. This is expected as photodetachment occurs from a nonbonding $2p\ \pi$ orbital. The large change in β from OH^- to $HOCO^-$ implies significant electronic structure changes which are not characteristic of cluster systems such as $OH^-(N_2O)_n$ which showed small changes in β relative to bare OH^-.[49] The value of β for $HOCO^-$ was also examined as a function of eKE, and showed very little dependence; it decreased slightly at larger eKE which is consistent with reduced resolution at higher eKE. The HOMO of *trans*-$HOCO^-$ as calculated at the CCSD(T)/6-311++G($3df$,$3pd$) level is shown in Fig. 4. This figure shows that there is significant electron density both on the C atom and on the terminal O atom, while there is less electron den-

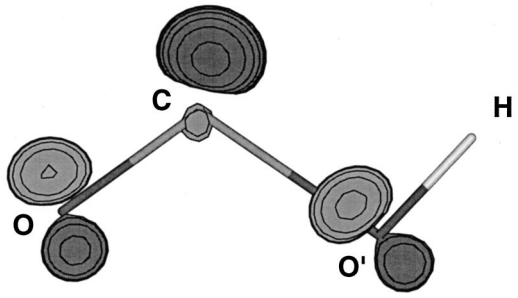

FIG. 4. Highest occupied molecular orbital (HOMO) for *trans*-$HOCO^-$ calculated at the CCSD(T)/6-311++G($3df$,$3pd$) level of theory.

sity on the O atom bonded to H. Similar results are seen for the HOMO of *cis*-$HOCO^-$. Thus, the electronic structure of this species cannot be characterized as a weak $OH^-(CO)$ complex and the striking difference between β values for OH^- and $HOCO^-$ provides strong evidence that $OH^-(CO)$ was not present in the ion beam and that ionic photodissociation did not play a role in these experiments.

C. Photofragment translational energy spectra

Figure 5 shows the neutral particle translational energy release distributions, $P(E_T)$, for DPD of $HOCO^-$ forming both $OH+CO+e^-$ and $H+CO_2+e^-$ products. Unlike the $N(E_T)$ distributions in Fig. 1, these $P(E_T)$ distributions are generated from the raw data by correcting for the finite DAF using Monte Carlo simulations as discussed in the Experiment. Both channels yield some products with relatively large translational energies. The spectrum for the $OH+CO$ products [reaction (1)] shows two regions; a large peak at very low kinetic energy extending out to 0.6 eV, and a small peak centered at 1.60 eV. The spectrum for the $H+CO_2$ products [reaction (2)] exhibits a peak at 0.53 eV and also has a peak at low E_T but shows no resolved features attributable to bending excitation of the CO_2 product as previously observed in studies of the DPD of HCO_2^-.[28] The origin of the peak at $E_T \approx 0$ eV was investigated in experiments at

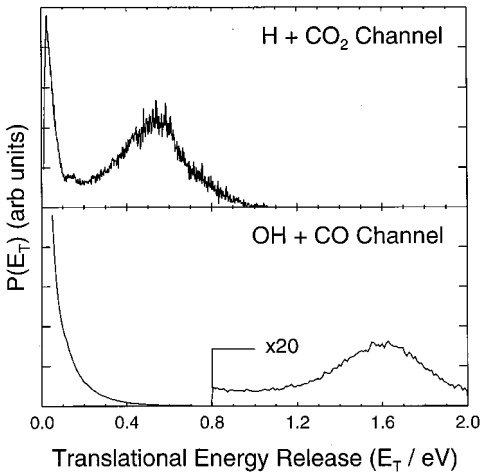

FIG. 5. Neutral particle translational energy distributions, $P(E_T)$, for dissociative photodetachment of $HOCO^-$ at 258 nm for the two available channels: $HOCO^- \rightarrow H+CO_2+e^-$ and $HOCO^- \rightarrow OH+CO+e^-$.

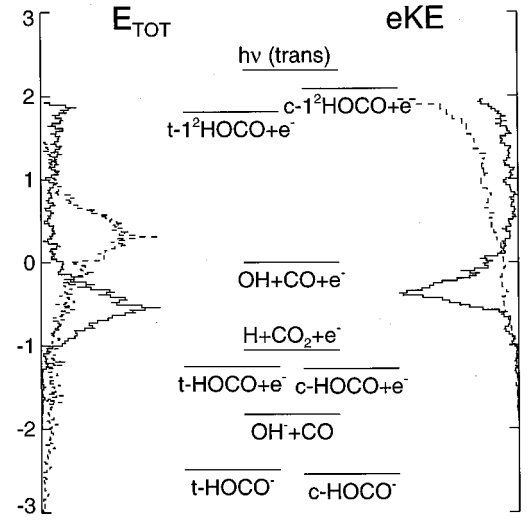

FIG. 6. Energetics diagram for DPD of $HOCO^-$. The $OH+CO+e^-$ exit channel is used as the reference. The position of the *cis* and *trans* ground state anions and neutrals are from the CCSD(T)/6-311++G($3df$,$3pd$) calculations in Table III. The position of the first excited states are from Ref. 25. The solid lines represent data correlated with $H+CO_2$ fragments, the dashed lines represent data correlated with $OH+CO$ fragments having $E_T > 0.5$ eV.

beam energies of both 4 and 7 keV, and no detectable change in the $P(E_T)$ distributions was observed, indicating that decomposition of energized radicals with lifetimes on the timescale of the 6–8 μs flight time to the detector was not occurring. The sharp peak at $E_T \approx 0$ eV in both channels is consistent with production of stable HOCO radicals by photodetachment of $HOCO^-$, as discussed above.

V. DISCUSSION

The photoelectron–photofragment coincidence experiments described here provide new experimental insights into the dissociation dynamics on the HOCO potential energy surface. In these experiments, the $HOCO^-$ molecular anion has been produced and characterized for the first time, and is found to undergo DPD to both $H+CO_2+e^-$ and $OH+CO+e^-$. There is also evidence for photodetachment yielding the stable HOCO radical in the ground electronic state. The experimental results are complemented by the first theoretical study of the structure and energetics of the $HOCO^-$ molecular anion. In conjunction with the extensive studies previously carried out on both ground and excited neutral HOCO potential energy surfaces, the anion theoretical predictions provide a basis for interpretation of the experimental observations.

To summarize the observations reported here, Fig. 6 shows an energetics diagram for DPD of both *cis*- and *trans*-$HOCO^-$, overlain with photoelectron and total energy spectra (where $E_{TOT} = eKE + E_T$ is generated from the coincidence data) for the two product channels. The solid lines represent data correlated with $H+CO_2$ fragments, and are consistent with the expected energetic onset of the $H+CO_2$ channel. The dashed lines represent data correlated with $OH+CO$ fragments having $E_T > 0.5$ eV, showing the total energy spectrum for only the diagonal feature at high E_T

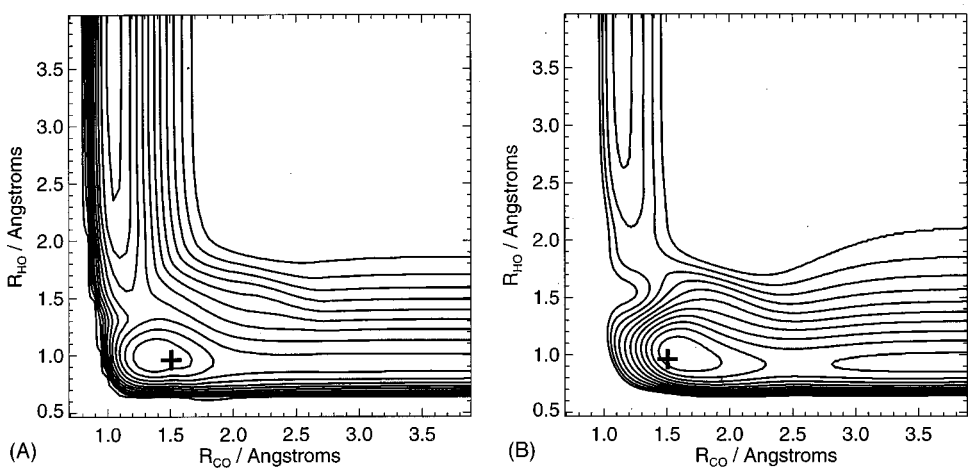

FIG. 7. Analytic potential energy surfaces for *trans*-HOCO from Ref. 26 along the H–O′ and O′–C coordinates, illustrating the relation of the calculated anion equilibrium geometry (marked as +) to the neutral potential energy surface. Frame A (right) shows a partially relaxed surface, where 3 other degrees of freedom (excluding the *cis*–*trans* isomerization angle) are optimized as a function of $r_{HO'}$ and $r_{O'C}$. Frame B (left) shows a surface with the geometry of the other coordinates frozen at the *trans*-$HOCO^-$ geometry, illustrating that vertical photodetachment leads to a configuration more removed from the equilibrium geometry.

[region 1 in Fig. 1(A)]. As seen in the correlation spectrum, some data attributable to false coincidences and hot bands extend significantly beyond the energetic limit for the OH + CO channel. In the following sections, a brief summary of the observed dissociation pathways and energetics is followed by an examination of the region of the neutral HOCO surface probed. Approximate product branching ratios for the $H+CO_2$, OH+CO and stable HOCO products are also presented.

The data obtained here show that DPD of $HOCO^-$ samples both product channels on the ground state $H+CO_2 \rightarrow OH+CO$ neutral potential energy surface, an excited state surface correlating to ground state products, and the stable HOCO radical as well. The theoretical calculations carried out show that both *cis*- and *trans*-$HOCO^-$ are covalently bound anions, and the calculated energetics are consistent with the experimental results. Furthermore, photoelectron angular distributions show that ionic photodissociation processes yielding $OH^- + CO$ followed by photodetachment of the OH^- product did not occur and that no evidence for weakly bound $OH^-(CO)$ clusters was observed.

The $P(E_T)$ spectra presented in Fig. 5 show that both exit channels are probed on the neutral potential surface. In the case of OH+CO, the two regions of the spectra indicate that more than one mechanism exists for dissociation, depending on where photodetachment of the anion occurs to the neutral potential surface. The high energy feature, peaking near $E_T = 1.6$ eV is consistent with dissociation on an excited state, while the broad feature peaking at 0 eV and tailing off at 0.6 eV results from unimolecular decomposition on the ground-state and false coincidences with stable HOCO radicals. The broad and relatively featureless spectrum for the $H+CO_2$ channel peaking at $E_T = 0.53$ eV is consistent with only one mechanism leading to dissociation along that coordinate. Both product channels show a peak near $E_T = 0$ eV. As discussed above, this feature is assigned to false coincidences with the stable HOCO radicals.

The $N(E_T, \text{eKE})$ correlation spectra presented in Fig. 1 yield the most interesting insights into the energetics and dynamics of the HOCO system. As mentioned previously, the diagonal lines marked by (I) in Fig. 1 represent the theoretical maximum energy for production of ground state $OH+CO+e^-$ and $H+CO_2+e^-$ products starting from both *cis*- and *trans*-$HOCO^-$. These limits match very well the energetic limits displayed by the features observed for both reaction pathways, with the largest discrepancy observed for the intermediate E_T feature in the $OH+CO+e^-$ spectrum ($0.05 \text{ eV} < E_T < 0.6$ eV). In this region, a significant fraction of the data extends over the energetic limit I, and will be further discussed below.

Region 1 of Fig. 1(A) exhibits a distinct diagonal energy-conservation cutoff, broad photoelectron and photofragment kinetic energy distributions and a significant repulsion between the photofragments. This is characteristic of direct DPD on a repulsive surface correlating to ground state products. Li and Francisco carried out high level *ab initio* calculations on the excited states of the HOCO radical, and found four low-lying excited states, two of $^2A''$ symmetry and two of $^2A'$ symmetry for both *cis*- and *trans*-HOCO.[25] The lowest of these, the $1\,^2A''$ state, has a vertical excitation energy of ≈4.2 eV. However, as shown by their study of the potential energy curves for this state, it rapidly drops in energy along the dissociation coordinate to ground state OH + CO products. Our observation of the high E_T associated with DPD on this repulsive state indicates that in the region of Franck–Condon overlap with the $HOCO^-$ anion this state has dropped to energies on the order of 1.6 eV above the dissociation asymptote.

Interpretation of the dynamics of dissociation on the ground state HOCO surface after photodetachment is aided by considering in more detail the potential energy surface for the $H+CO_2 \rightarrow OH+CO$ reaction. Muckerman and coworkers have recently published a detailed six-dimensional surface for this reaction that allows examination of the energetics along a number of degrees of freedom.[26] In Fig. 7, two representations of the potential energy surface for *trans*-HOCO along the H–O and O–C bonds are shown. Figure 7(A) is a partially relaxed surface, where the other degrees of freedom are optimized within constraints following Ref. 26. Figure 7(B) is a surface in which the H–O′ and O′–C bonds are allowed to vary while the other degrees of freedom are fixed in the *trans*-$HOCO^-$ anion geometry. The many body expansion used to fit these curves causes the O′–C bond

length at the minimum of the HO′CO well to be significantly longer than calculated, so they have been offset to put the minimum of the HOCO well at the O′–C and H–O′ bond lengths reported in Table I and in the work of Yu *et al.*[26] The crosses placed on these surfaces represent the equilibrium *trans*-$HOCO^-$ geometry, indicating the region of Franck–Condon overlap in photodetachment to the neutral surface. Both figures show that photodetachment occurs into the region of the HOCO well, indicating that the observation of a significant stable HOCO fraction is not surprising, while the dissociation channels may be expected to exhibit features consistent with unimolecular dissociation from the HOCO well.

The dynamics observed in the $H+CO_2+e^-$ channel, where $P(E_T)$ is peaked at 0.53 eV, are consistent with unimolecular decomposition of excited HOCO radicals out of the well and over the barrier to the $H+CO_2$ products, ≈0.1 eV above the OH+CO asymptote.[26] After crossing the barrier, 1.06–1.36 eV above the asymptotic $H+CO_2$ products, a significant amount of energy appearing in product translation is expected.[26] Unimolecular dissociation over a barrier typically leads to $P(E_T)$ distributions peaked away from 0 eV,[50] and it is not surprising to find in this case that a significant fraction of the barrier height ends up in internal degrees of freedom given the significant change in geometry from HOCO to $H+CO_2$ products. It is interesting to note that the peak in this distribution is similar to that previously observed in the DPD of the formate anion, HCO_2^-.[28] In the case of HCO_2^-, however, predissociation sequence bands were observed in the correlation spectrum related to production of a distribution of product CO_2 bending vibrations from each bend-excited HCO_2 predissociative state. In the DPD of $HOCO^-$, vibrational excitation of the product CO_2 is also expected since there is a significant change in OCO bond angle from either *cis*- or *trans*-$HOCO^-$ ($\theta \approx 110°$) to linear CO_2. The lack of observed structure in the current experiments probably arises from increased CO_2 product rotation. In the DPD of HCO_2^-, very little rotation is expected since HCO_2 is planar and only limited orbital angular momentum is involved in the departure of the H atom from the carbon atom in the CO_2 product for dissociation in C_{2v} symmetry.[28] However, in the DPD of either *cis*- or *trans*-$HOCO^-$, momentum transfer to the CO_2 product occurs essentially side-on to one of the O atoms yielding significant CO_2 rotation, resulting in a broader, unresolved E_T spectrum.

The dynamics observed on the ground state HOCO surface for the $OH+CO+e^-$ channel are also consistent with photodetachment into the region of the HOCO well. The excited-state dissociation products, seen at large E_T, were discussed previously, and here we focus on the two features seen below $E_T=0.6$ eV in the correlation spectrum. There is predicted to be only a small barrier (none on the *trans*-HOCO surface and only 0.11 eV on the *cis*-HOCO surface) in unimolecular decomposition to OH+CO products,[21,26] so it is expected to find a $P(E_T)$ peaking near 0 eV for this type of simple bond rupture reaction. A significant amount of data in the $E_T=0.05-0.5$ eV range for this channel is seen to lie beyond the energetic limit I. This partially arises from the limited ≈250 meV eKE resolution for these high energy

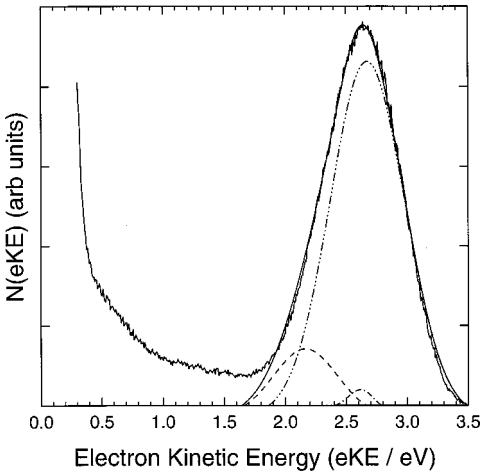

FIG. 8. The overall photoelectron spectrum for $HOCO^-$ observed in this experiment, representing photoelectrons recorded in coincidence with one or more neutral particles. The solid line shows a fit to the data with three components given by the dashed line curves representing, in order of increasing energy, the $OH+CO+e^-$, $H+CO_2+e^-$, and $HOCO+e^-$ channels.

electrons (see the OH^- spectrum shown in Fig. 2) and also contains hot band contributions from vibrationally excited $HOCO^-$ anions. The branching ratio between stable HOCO and dissociation products is expected to be very sensitive to vibrational excitation in the parent anion. Given the lack of a vibrationally resolved photoelectron spectrum, a detailed estimate of the anion temperature is not available. However, polyatomic anions in supersonic expansion ion sources of the type used here typically exhibit vibrational temperatures in the 200–500 K range.

A final aspect of considerable interest is the branching ratio between stable HOCO and the $H+CO_2$ and OH+CO products. This branching ratio should in principle be obtainable from either the photoelectron spectra or the neutral particle spectra. The difficulty found in extracting the branching ratio from the neutral particle spectra involves the very low detection efficiency for the $H+CO_2$ products and the overlapping $P(E_T)$ distribution for the low energy OH+CO products and the stable HOCO radicals at $E_T=0$ eV. For this reason, we calculate an approximate branching ratio by deconvolution of the overall photoelectron spectrum using the spectra for the individual channels shown in Fig. 2.

Figure 8 shows the N(eKE) spectrum recorded in coincidence with one or more neutral(s) striking the particle detector, and contains data from both dissociation channels and stable HOCO radicals as well. It is thus different from the differential N(eKE) spectra for the dissociation channels shown in Fig. 2. A brief comment on the energetic implications of this overall N(eKE) spectrum is in order. Given the 4.80 eV photon energy and assuming that only one isomer contributes to the photoelectron spectrum, the peak in this spectrum indicates that $HOCO^-$ has a vertical detachment energy (VDE) of 2.18 ± 0.02 eV. The observed VDE in the photoelectron spectrum in Fig. 8 of 2.18 eV is 0.88 and 0.75 eV larger than the calculated AEA for the *trans* and *cis* isomers, respectively. This is consistent with a significant change in geometry from the anion to the neutral, and the

creation of internally excited neutrals on the ground state surface that may undergo subsequent unimolecular decomposition.

The three functions fit to Fig. 8 correspond to functional forms taken from the $OH+CO+e^-$ spectrum for $E_T > 0.05$ eV, the $H+CO_2+e^-$ spectrum and the $HOCO+e^-$ spherically gated spectrum (all shown in Fig. 2). The areas of these three features (with the $OH+CO+e^-$ spectrum at the lowest eKE and the $H+CO_2+e^-$ spectrum being the smallest component) gives a branching ratio of 83% HOCO, 13% $OH+CO$, and 4% $H+CO_2$. However, as discussed previously, the CO_2 neutrals at low E_T will be indistinguishable from stable HOCO radicals. Monte Carlo simulations indicate that 37% of the CO_2 fragments from $H+CO_2$ dissociation are expected to appear in the $HOCO+e^-$ component. This gives a revised branching ratio of 81% HOCO, 13% $OH+CO$, and 6% $H+CO_2$. The production of a significant amount of stable HOCO radicals is not surprising given the Franck–Condon overlap with the neutral surface discussed above. However, the 2:1 inferred preponderance of the $OH+CO$ channel relative to the $H+CO_2$ channel is surprising as discussed below. It must be stressed that these numbers are approximate given the low eKE resolution at the relatively high photoelectron kinetic energies, with an estimated error of approximately 20%. The large yield of stable HOCO radicals found explains the significant false-coincidence contribution from $HOCO+e^-$ events to the $H+CO_2+e^-$ and $OH+CO+e^-$ spectra.

These branching ratios can be compared to those predicted by RRKM calculations[51] for thermal decomposition from the HOCO well employing transition state structures, energies, and frequencies as given by Muckerman and co-workers.[26] For the $OH+CO$ products of the $H+CO_2 \rightarrow OH+CO$ reaction, good agreement has previously been observed between RRKM theory and experimental lifetime determinations,[10] consistent with IVR occurring in the $HOCO^+$ complex prior to unimolecular decomposition. At energies well above the transition states, which is the energetic region probed in this study, RRKM calculations yield a branching ratio of 6.7 in favor of $OH+CO$ over $H+CO_2$, significantly larger than the experimental results. An additional point to be made from the calculations is that even at the energetic threshold of the $H+CO_2$ transition state, a rate constant of 7×10^{11} s^{-1} is determined, yielding an average lifetime for HOCO of only 2 ps. Thus we do not believe that the feature assigned to stable HOCO radicals is in fact metastable, consistent with the experiments carried out at different beam energies as discussed above.

The discrepancy between the branching ratio calculated from the data and RRKM calculations is surprising. An important consideration is that the RRKM calculations do not take into account effects arising from the fact that the Franck–Condon factors for photodetachment to the ground state HOCO surface will produce a nonthermal distribution of initial product states. In addition, contributions from tunneling were not included. These will be more important for the energetically favored $H+CO_2$ channel. Future work on this reaction such as detailed wavepacket dynamics calculations could aid in explaining the discrepancies between RRKM calculations and observed branching fractions. Such calculations should provide a direct prediction not only of the dissociation product channel branching ratios, but also the fraction of stable HOCO radicals produced by photodetachment.

VI. CONCLUSIONS

The DPD dynamics of $HOCO^-$ were studied by photoelectron photofragment coincidence spectroscopy. After photodetachment at 258 nm, stable HOCO radicals and both $OH+CO$ and $H+CO_2$ products were observed. The $H+CO_2$ results are consistent with unimolecular dissociation of HOCO over a barrier and are characterized by a featureless photoelectron–photofragment correlation spectrum consistent with significant CO_2 product rotation, in contrast to the vibrationally resolved dynamics previously observed for the HCO_2 radical. The $OH+CO$ channel exhibits more complicated behavior. A high E_T channel was observed corresponding to direct DPD on a repulsive electronically excited state correlating to ground state $OH+CO+e^-$. A low E_T channel, consistent with unimolecular dissociation of the energized HOCO species was also observed. The $P(E_T)$ for this channel is found to peak near $E_T=0$ eV, consistent with little or no barrier in the exit channel.

The photoelectron spectra and photoelectron angular distributions measured mark the first experimental characterization of the $HOCO^-$ molecular anion, and reveal that there is no weakly bound $OH^-(CO)$ complex formed. Supporting *ab initio* calculations on the $HOCO^-$ and HOCO *cis*- and *trans*-species provided energetics that are in excellent accord with the experimental results. In addition, the structural information obtained when compared to the analytic potential energy surface of Ref. 26 provides an understanding of the observed ground-state dynamics. Thanks to the geometry of the $HOCO^-$ molecular anion, the data presented here provide important new experimental insights into the potential surface governing the $OH+CO \rightarrow H+CO_2$ reaction. Photodetachment occurs into the region of the HOCO radical well on the ground state surface and both exit channels are accessed in unimolecular dissociation. Higher resolution experiments at lower photon energies should allow improvement of the experimental energetics and branching ratios in the future. In addition, studies of the DOCO radical will be valuable. It will clearly be of great interest to carry out multidimensional dynamics calculations on this system in the future to compare with these experimental results.

ACKNOWLEDGMENTS

This work was supported by the Department of Energy (DOE) under Grant No. DE-FG03-98ER14879. J.S.F. thanks the NASA Jet Propulsion Laboratory for ample computing resources to conduct this research. The NASA Office of Space Science and Applications sponsors the Jet Propulsion Laboratory Supercomputing Project. T.G.C. is supported under AFOSR Grant No. F49620-000-10-010. The authors thank Dr. H.-G. Yu and Dr. J. Muckerman for providing the functional form of the HOCO neutral potential energy surface described in Ref. 26.

[1] C. T. Bowman, in *Fossil Fuel Combustion*, edited by W. Bartok and A. F. Sarofim (Wiley, New York, 1991).
[2] R. P. Wayne, *Chemistry of Atmospheres*, 2nd ed. (Clarendon, Oxford, 1991).
[3] M. Alagia, N. Balucani, P. Casavecchia, D. Stranges, and G. G. Volpi, J. Chem. Phys. **98**, 8341 (1993).
[4] M. J. Frost, P. Sharkey, and I. W. M. Smith, Faraday Discuss. **91**, 305 (1991).
[5] G. W. Flynn and R. E. Weston, Jr., J. Phys. Chem. **97**, 8116 (1993).
[6] M. Brouard, D. W. Hughes, K. S. Kalogerakis, and J. P. Simons, J. Phys. Chem. A **102**, 9559 (1998).
[7] M. Brouard, D. W. Hughes, K. S. Kalogerakis, and J. P. Simons, J. Chem. Phys. **112**, 4557 (2000).
[8] N. F. Scherer, C. Sipes, R. B. Bernstein, and A. H. Zewail, J. Chem. Phys. **92**, 5239 (1990).
[9] S. K. Shin, C. Wittig, and W. A. Goddard, J. Phys. Chem. **95**, 8048 (1991).
[10] S. I. Ionov, G. A. Brucker, C. Jaques, L. Valachovic, and C. Wittig, J. Chem. Phys. **99**, 6553 (1993).
[11] M. I. Lester, B. V. Pond, M. D. Marshall, D. T. Anderson, L. B. Harding, and A. F. Wagner, Faraday Discuss. **118**, 373 (2001).
[12] T. J. Sears, W. M. Fawzy, and P. M. Johnson, J. Chem. Phys. **97**, 3996 (1992).
[13] J. T. Petty and C. B. Moore, J. Mol. Spectrosc. **161**, 149 (1993).
[14] M. E. Jacox, J. Chem. Phys. **88**, 4598 (1988).
[15] T. V. Duncan and C. E. Miller, J. Chem. Phys. **113**, 5138 (2000).
[16] B. Ruscic and M. Litorja, Chem. Phys. Lett. **316**, 45 (2000).
[17] M. Aoyagi and S. Kato, J. Chem. Phys. **88**, 6409 (1988).
[18] K. Kudla, G. C. Schatz, and A. F. Wagner, J. Chem. Phys. **95**, 1635 (1991).
[19] D. C. Clary and G. C. Schatz, J. Chem. Phys. **99**, 4578 (1993).
[20] M. I. Hernandez and D. C. Clary, J. Chem. Phys. **101**, 2779 (1994).
[21] K. S. Bradley and G. C. Schatz, J. Chem. Phys. **106**, 8464 (1997).
[22] F. N. Dzegilenko and J. M. Bowman, J. Chem. Phys. **108**, 511 (1998).
[23] D. H. Zhang and J. Z. H. Zhang, J. Chem. Phys. **103**, 6512 (1995).
[24] D. A. McCormack and G. J. Kroes, J. Chem. Phys. **116**, 4184 (2002).
[25] Y. Li and J. S. Francisco, J. Chem. Phys. **113**, 7963 (2000).
[26] H.-G. Yu, J. T. Muckerman, and T. J. Sears, Chem. Phys. Lett. **349**, 547 (2001).
[27] E. H. Kim, S. E. Bradforth, D. W. Arnold, R. B. Metz, and D. M. Neumark, J. Chem. Phys. **103**, 7801 (1995).
[28] T. G. Clements and R. E. Continetti, J. Chem. Phys. **115**, 5345 (2001).
[29] K. A. Hanold, C. R. Sherwood, M. C. Garner, and R. E. Continetti, Rev. Sci. Instrum. **66**, 5507 (1995).
[30] K. A. Hanold, A. K. Luong, T. G. Clements, and R. E. Continetti, Rev. Sci. Instrum. **70**, 2268 (1999).
[31] J. A. Davies, J. E. LeClaire, R. E. Continetti, and C. C. Hayden, J. Chem. Phys. **111**, 1 (1999).
[32] L. S. Alconcel, H. J. Deyerl, M. DeClue, and R. E. Continetti, J. Am. Chem. Soc. **123**, 3125 (2001).
[33] C. R. Sherwood and R. E. Continetti, Chem. Phys. Lett. **258**, 171 (1996).
[34] B. L. Peko and T. M. Stephen, Nucl. Instrum. Methods Phys. Res. B **171**, 597 (2000).
[35] M. J. Frisch, G. W. Trucks, H. B. Schlegel *et al.*, GAUSSIAN 98, Revision A.7, Gaussian, Inc., Pittsburgh, PA, 1998.
[36] G. E. Scuseria, C. L. Janssen, and H. F. Schaefer III, J. Chem. Phys. **89**, 7382 (1988).
[37] R. Krishnan, J. S. Binkley, R. Seeger, and J. A. Pople, J. Chem. Phys. **72**, 650 (1980).
[38] J. S. Francisco, J. Chem. Phys. **107**, 9039 (1997).
[39] P. A. Schulz, R. D. Mead, P. L. Jones, and W. C. Lineberger, J. Chem. Phys. **77**, 1153 (1982).
[40] M. W. Chase, Jr., C. A. Davies, J. R. Downy, Jr., D. J. Frurip, R. A. McDonald, and A. N. Syverud, *JANAF Thermochemical Tables*, Suppl. 1 ed. (American Institute of Physics, New York, 1985).
[41] K. A. Hanold and R. E. Continetti, Chem. Phys. **239**, 493 (1998).
[42] H.-J. Deyerl, A. K. Luong, T. G. Clements, and R. E. Continetti, Faraday Discuss. **115**, 147 (2000).
[43] H.-J. Deyerl, T. G. Clements, A. K. Luong, and R. E. Continetti, J. Chem. Phys. **115**, 6931 (2001).
[44] R. N. Zare, Mol. Photochem. **4**, 1 (1972).
[45] L. M. Smith and D. R. Keefer, J. Quant. Spectrosc. Radiat. Transf. **39**, 367 (1988).
[46] R. N. Strickland and D. W. Chandler, Appl. Opt. **30**, 1811 (1991).
[47] C. Bordas, F. Pauling, H. Helm, and D. L. Huestis, Rev. Sci. Instrum. **67**, 2257 (1996).
[48] H.-J. Deyerl, L. S. Alconcel, and R. E. Continetti, J. Phys. Chem. A **105**, 552 (2001).
[49] J. B. Kim, P. G. Wenthold, and W. C. Lineberger, J. Chem. Phys. **108**, 830 (1998).
[50] T. Baer and W. L. Hase, *Unimolecular Reaction Dynamics* (Oxford, New York, 1996).
[51] W. L. Hase and D. L. Bunker, QCPE **11**, 234 (1973).
[52] M. J. Frisch, H. F. Schaefer III, and J. S. Binkley, J. Phys. Chem. **89**, 2192 (1985).